n -Alkylsiloxanes: From Single Monolayers to Layered Crystals. The Formation of Crystalline Polymers from the Hydrolysis of n -Octadecyltrichlorosilane

ARTICLE *in* JOURNAL OF THE AMERICAN CHEMICAL SOCIETY · APRIL 1997

Impact Factor: 12.11 · DOI: 10.1021/ja963284p

n-Alkylsiloxanes: From Single Monolayers to Layered Crystals. The Formation of Crystalline Polymers from the Hydrolysis of *n*-Octadecyltrichlorosilane

A. N. Parikh,[‡,§] M. A. Schivley,[†] E. Koo,[‡] K. Seshadri,[†] D. Aurentz,[†] K. Mueller,[†] and D. L. Allara*[,†,‡]

Contribution from the Departments of Chemistry and Materials Science & Engineering, Pennsylvania State University, University Park, Pennsylvania 16802

Received September 18, 1996[⊗]

Abstract: Formation of a new class of layered, microcrystalline polymers from a simple hydrolytic polycondensation of *n*-alkyltrichlorosilanes in water is demonstrated. The structure of the polymeric condensate, determined from a combination of spectroscopic, diffraction, and thermal analysis techniques, consists of highly uniform, pillared microcrystallites in which the inorganic siloxy backbones are present in periodic layers, each containing a monomolecular layer of intercalated water, separated by crystalline assemblies of alkyl chains. The alkyl-chain organization shows a remarkable resemblance to that in highly organized, self-assembled monolayers formed from the precursor silane molecules on hydrophilic substrates and this parallel lends support to the critical importance of water in monolayer self-assembly of silanes.

1. Introduction

There has been considerable interest recently in the connection between the structural organization and the formation mechanism of self-assembled monolayers of *n*-alkylsiloxanes on solid surfaces.[1] Recently it has been proposed, with experimental support, that the highest degree of film organization is attained when an ultrathin, physisorbed layer of water is present at the film−substrate interface during the film formation process.[1c,d] Under these conditions, the mechanism of film formation involves the self-organization of a quasi-two-dimensional (2-D) assembly of hydrolyzed precursors of the initial *n*-alkyltrifunctional silanes, namely alkyltrihydroxysilanes [*n*-C_nH_{2n+1}-$Si(OH)_3$], which in the initial low-coverage stages of the film are laterally mobile at the film−water interface, in a manner analogous to typical surfactant Langmuir films at the surface of bulk water. In the subsequent, high-coverage stages, the film undergoes cross-linking via intermolecular condensation of −SiOH groups on neighboring molecules to form siloxane or Si−O−Si bonds. A key feature of this mechanism is the parallel between the structural phases formed from typical alkyl-chain surfactant molecules and analogous alkyltrihydroxysilane species; the central example is the comparison of Langmuir films of *n*-$C_{18}H_{37}CO_2H$ and self-assembled monolayers (SAMs) of hydrolyzed *n*-$C_{18}H_{37}SiCl_3$ (*n*-octadecyltrichlorosilane; OTS) on hydrophilic surfaces.[1c] This analogy suggests that a variety of highly organized 3-D phase structures, based on periodic mimics of the varieties of quasi-2-D monolayer assemblies known for typical monomeric surfactants,[2] should be achievable during the bulk hydrolysis of trifunctional alkylsilanes. In fact, recent evidence hints that organized 3-D structures do in fact exist. Thompson and Pemberton[3] report Raman spectra which show that a gel formed from the hydrolysis of (OTS) contains conformationally ordered alkyl chains. Similarly, Gao and Reven report[4] that an OTS hydrolysis product exhibits magic angle spinning NMR (MAS-NMR) spectra typical of conformationally ordered chains. In neither of these two studies was the insoluble hydrolysis product characterized in further detail, leaving open the question of the specific types of structures formed. Independent of the above reports, we have been carrying out extensive characterization of hydrolyzed bulk alkylsiloxanes in order to specifically identify the possible existence of parallels with monolayer self-assembly, particularly with respect to the role of interfacial water films. In this report, we present extensive characterization evidence, including infrared (IR) and Raman spectroscopy, wide angle and small angle X-ray diffraction (WAXRD and SAXRD), nuclear magnetic resonance (NMR), and thermal gravimmetric analysis (TGA), which shows that simple hydrolysis can spontaneously lead to the formation of layered crystals constituted from stacks of head-to-head bilayers in which each layer is comprised of conformationally ordered alkyl chains. Further, our evidence for the specific case of polymerized *n*-octadecylsiloxane (poly-ODS or PODS) shows that each of the individual layers exhibits a structure virtually identical to that of a single self-assembled monolayer of ODS on a smooth planar substrate, e.g., SiO_2, and that the siloxy−siloxy interlayer regions contain monolayer quantities of water molecules, similar to what is believed to exist at the film−substrate interface in substrate-supported, self-assembled ODS monolayers. This evidence establishes a strong parallel between the 2- and 3-D self-assembly processes of *n*-alkylsiloxanes and the critical importance of water in the assembly mechanisms. Further, these layered siloxanes add a new type of structure to the extensive silsesquioxane structures which have been discovered for the hydrolysis of a variety of organosilanes from tetraalkoxysilanes[5] to various alkyl-substi-

[†] Department of Chemistry.
[‡] Department of Materials Science & Engineering.
[§] Present address: Los Alamos National Laboratory, Chemical Science & Technology Division, Los Alamos, NM 87545. E-mail: parikh@lanl.gov.
[⊗] Abstract published in *Advance ACS Abstracts,* March 1, 1997.

(1) (a) Silberzan, P.; Leger, L.; Ausserré, D.; Benattar, J. J. *Langmuir* **1991**, *7*, 1647−1651. (b) Tripp, C. P.; Hair, M. L. *Langmuir* **1992**, *8*, 1120−1126. (c) Allara, D. L.; Parikh, A. N.; Rondelez, F. *Langmuir* **1995**, *11*, 2357−2360. (d) Parikh, A. N.; Allara, D. L.; BenAzouz, I.; Rondelez, F. *J. Phys. Chem.* **1994**, *98*, 7577−7590.

(2) See, for example: Kaler, E. W.; Murthy, A. K.; Rodriguez, B. E.; Zasadzinski, J. A. N. *Science* **1989**, *245*, 1371−1374 and selected references cited therein.

(3) Thompson, W. R.; Pemberton, J. E. *Langmuir* **1995**, *11*, 1720−1725.

(4) Gao, W.; Reven, L. *Langmuir* **1995**, *11*, 1860−1863.

S0002-7863(96)03284-2 CCC: $14.00

tuted ones.[6] Finally, we note the strong correspondence between the molecular-level structural attributes of these layered organosiloxanes and the well-known layered crystals of other organic−inorganic compounds[7] such as alkylzirconium phosphates and phosphonates, $Zr(O_3POR)_2$ and $Zr(O_3PR)_2$, respectively,[8,9] compounds of considerable interest because of their unique materials properties.[10]

2. Experimental Section

2.1. Materials and Preparation. Small amounts of OTS (Aldrich) were vacuum distilled (7.5×10^{-2} Torr, ∼155 °C) immediately prior to each use. Water was deionized (>18 MΩ cm resistivity) and scrubbed of organic contaminants in a Milli-RO, milli-Q purification system (Millipore, Bedford, MA). All solvents were reagent grade quality (Aldrich) and used as received. All glassware was cleaned thoroughly prior to each use with chromosulfuric acid followed by water rinsing and air drying at ∼110 °C.

The poly(octadecylsiloxane) (PODS) samples were prepared by dropwise addition of OTS from a glass pipette into a large stoichometric excess of water held under constant stirring at ∼5 °C. Upon the initial precipitation, the material is suspended in the solution as a fine white suspension but after about 15 min rises to the surface as a flaky material. After standing for ∼30−45 min, the precipitate was collected by suction filtration, thoroughly washed with water to remove residual hydrochloric acid as monitored by approach to a neutral pH, and then dried for several days under vacuum at room temperature. The collected white powder was stored in a dry atmosphere until use. The compound appeared highly insoluble in all typical organic solvents up to their boiling points including hexane, ethanol, trichlorobenzene, and chloroform with the exception of acetone which allowed solubilization of small amounts of material upon vigorous stirring for several hours.[11] A density of 0.89 g/cm^3 was determined by immersion in different density liquids. Differential scanning calorimetry (heating rate of 20 °C/min) showed the presence of a sharp exotherm at 84 °C which is attributed to alkyl-chain melting, as confirmed by infrared spectroscopy observations.[12] Above this transition no further heat flow changes were noted. Elemental analyses (average of six samples, all constant within 1 wt %) gave the following: C, 70.15; H, 11.84; Si, 7.28; O, 10.73% with a corresponding stoichiometry of $C_{18}H_{36.15}Si_{0.797}O_{2.065}$. While this value is generally close to the formulas $C_{18}H_{37}Si_{1.0}O_{1.5}$ and $C_{18}H_{39}Si_{1.0}O_{2.5}$ which correspond to the theoretical values for fully cross-linked octadecylsiloxane moieties with incorporation of no water and one water, respectively, the observed Si content is marginally lower than estimated.

2.2. Characterization. 2.2.1. Thermal Gravimetric Analysis. Thermally induced weight changes were monitored (Seiko TG/DTA 320u) under flowing argon or nitrogen environments in order prevent oxidative combustion at elevated temperatures. The measurements were made over the range 30−800 °C at a heating rate of 5 °C/min, and data were acquired at ∼0.03° intervals.

2.2.2. X-ray Diffraction. Wide angle diffraction patterns were obtained on a Rigaku Geigerflex diffractometer (with Dmax-B controller and a vertical goniometer) using Cu Kα (1.541 871 Å) radiation and a graphite monochromator. The samples were prepared by packing ∼5 mg of solid in a standard cavity mount. Digital data were obtained for a 2θ range 5−70° at an angular resolution of 0.02° with a total counting time of 2 h. Analyses of the data were performed using standard curve-fitting programs.

Details of the small angle X-ray diffraction apparatus used can be found elsewhere.[13] Measurements were performed with Cu Kα radiation with the X-ray generator operating at 40 kV and 35 mA. After passing through the monochromator (Ni-coated mirrors) the beam was collected at the detector with a 2.19 mrad (2θ) full width at half-maximum. A two-dimensional solid-state X-ray detector interfaced to a personal computer was used for data acquisition and analysis, and the sample to detector distance was maintained at 12 cm. Typical counting times were 6 h. The sample was prepared by pressing the solid powder in the form of <2 mm thickness pellets under ∼(10−20) × 10^3 psi.

2.2.3. Infrared Spectroscopy. Infrared transmission spectra were collected using a Fourier transform spectrometer (Bomem Model MB-100, Québec, Canada) operating at 2 cm^{-1} resolution with an unpolarized beam striking the sample at normal incidence. The beam diameter was controlled at 6 mm by an aperture placed adjacent to the sample. The resulting interferograms from multiple, co-added scans were Fourier transformed with triangular apodization and zero-filling to increase the point density by a factor of 4, for accurate determination of peak positions. The sample consisted of essentially transparent pellets prepared by pressing mechanically homogenized mixtures of the dried precipitate with nominally dehydrated pure KBr in calculated quantities. The spectra were referenced against the spectra obtained for air or blank KBr pellets under otherwise identical spectrometer condition and geometry. All spectra are reported in transmission absorbance units, defined as $-\log(T/T_o)$, where T and T_o are the emission power spectra of each sample and reference, respectively. For selected samples, temperature-dependent spectra were generated at intervals of 25.0 °C over a range of sample temperatures between 25 and 200 °C with the sample temperature held constant to within ±0.5 °C. In order to prevent oxidative degradation of the sample, the spectrometer during the latter measurements was purged with nitrogen. Absorption spectra were calculated using a reference spectrum collected at room temperature, as described above.

2.2.4. Nuclear Magnetic Resonance. A cross-polarization magic angle spinning (CP-MAS) ^{13}C NMR spectrum as well as single-pulse ^{29}Si MAS NMR spectrum with proton decoupling during acquisition were acquired on a Chemagnetics CMX-300 spectrometer operating at resonance frequencies of 59.072 449 MHz for ^{29}Si and 74.781 093 MHz for ^{13}C. All experiments were performed using a 7.5 mm rotor in a Chemmagnetics pencil probe and spinning speeds varied from approximately 2.5 to 2.8 kHz. Cross polarization was achieved by satisfying the Hartman−Hahn matching condition and employing a contact time of 2 ms for ^{1}H and ^{13}C. The ^{29}Si chemical shifts were referenced to tetramethylsilane (TMS) by using a second standard of tetrakis(trimethylsilyl)silane (the upfield peak occuring at −135.4 ppm). The ^{13}C chemical shifts also were referenced to TMS via a secondary standard of hexamethylbenzene (the isotropic peak occurring at 132.2 ppm).

2.2.5. Raman Spectroscopy. Raman spectra were obtained using a coherent Kr^+ ion laser, Model 3000K, operated at 530.9 nm wavelength in TEM_{00} with an ∼40 mW output. The laser beam was focused onto the sample, packed into a quartz tube, at an angle of <30° from the surface normal. After collection, the scattered light was focused onto the slit of a Spex Model 1404 scanning double mono-

(5) (a) Brinker, C. J.; Scherer, G. W. *Sol-Gel Science: The Physics and Chemistry of Sol-Gel Processing*; Academic Press: San Diego, CA, 1990. (b) Iler, R. K. *The Chemistry of Silica*; Wiley: New York, 1979. (c) Klein, L. C., Ed. *Sol-Gel Technology for Thin Films, Fibers, Preforms, Electronics, and Specialty Shapes*; Noyes Pub.: Park Ridge, NJ, 1988.

(6) For a recent review, see: (a) Wen, J.; Wilkes, G. L. *Chem. Mater.* **1996**, *8*, 1667−1681 and references therein. See also: (b) Baney, R. H.; Itoh, M.; Sakakibara, A.; Suzuki, T. *Chem. Rev.* **1995**, *95*, 1409−1430 and selected references therein. (c) Loy, D. A.; Shea, K. J. *Ibid.* **1995**, *95*, 1431−1442.

(7) (a) See, for example a review: Alberti, G.; Constantino, U. *Intercalation Chemistry*; Academic Press: New York, 1982; pp 147−180. See also: (b) Cao, G.; Hong, H.-G.; Mallouk, T. E. *Acc. Chem. Res.* **1992**, *25*, 420−427. (c) Mallouk, T. E.; Lee, H. *J. Chem. Educ.* **1990**, *67*, 829−834.

(8) Yamanaka, S. *Inorg. Chem.* **1976**, *15*, 2811.

(9) (a) Alberti, G.; Casciola, M.; Costantino, U.; Vivani, R. *Adv. Mater.* **1996**, *8*, 291−303 and references therein. (b) Alberti, G.; Constantino, U.; Allulli, S.; Tomassini, N. *J. Inorg. Nucl. Chem.* **1978**, *40*, 1113.

(10) (a) Alberti, G. In *Recent Developments in Ion Exchange*; Willliams, P. A., Hudson, M. J., Eds.; Elsevier Applied Science: New York, 1987. (b) Clearfield, A. In *Design of New Materials*; Cocke, D. L., Clearfield, A., Eds.; Plenum Press: New York, 1988. (c) Johnson, J. W.; Brody, J. F.; Alexander, R. M.; Pilarski, B.; Katrizsky, A. R. *Chem. Mater.* **1990**, *2*, 198−201. (d) Lee, H.; Kepley, L. J.; Hong, H.; Mallouk, T. E. *J. Am. Chem. Soc.* **1988**, *110*, 618−620.

(11) Since only small amounts of the acetone soluble fraction were available it was not characterized further. However, work is now in progress to characterize such soluble fractions as a function of chain lengths and preparation conditions.

(12) Details of the low-temperature thermal transistions of poly(*n*-alkylsiloxanes) will be reported elsewhere.

(13) Gupta, A.; Simpson, D. M.; Harrison, I. R. *J. Appl. Polym. Sci.* **1993**, *50*, 2085−2093.

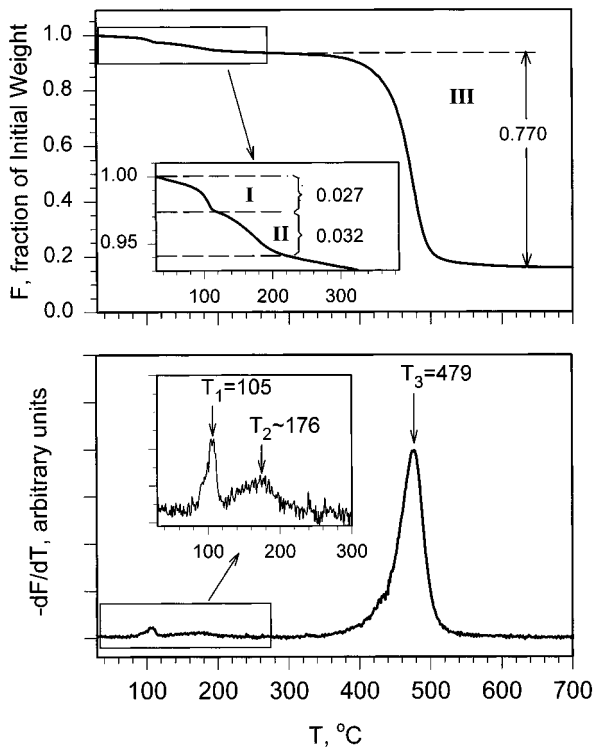

Figure 1. Thermal gravimetric scan of PODS. The weight loss trace in the top plot is divided into separate regions. The corresponding break points correspond to the maxima in the derivative trace shown in the lower plot.

chromator, equipped with 1800 grooves/mm gratings, and the diffracted light detected using a thermoelectrically cooled Hamamatsu R928 photomultiplier tube. The monochromator entrance and exit slits and the center slits were set at nominal values of 700 and 1400 μm, respectively, to yield an effective band pass of 5 cm^{-1}. The data were collected at 1 cm^{-1} steps with 1 s integration intervals.

3. Results

3.1. Thermal Gravimetric Analysis. The plots in Figure 1 show the presence of three discernible weight loss regions: (I) a small transition at ~105 °C, (II) a second small transition at ~176 °C, and (III) a large transition at ~479 °C. The first two transitions are assigned primarily to the loss of physically bound water. While the lowest temperature transition is clearly consistent with this type of loss, presumably representing entrapped water within the siloxy network, the higher temperature transition could also include the onset of some water release from subsequent condensation reactions between unreacted SiOH groups (see section 3.4) forming new SiOSi cross-links. On the basis of an average molecular weight of 309 (calculated from the observed elemental analysis; see section 2.1), the observed 5.9% weight loss, determined as shown in Figure 5a, corresponds almost exactly to one water molecule per alkylsiloxane molecule. The slowly decreasing slope leading to the third transition region likely signals further loss of water by the above silanol condensation reactions. However, since the slope merges into that of the large third transition region, it is not possible to quantitate any condensation loss. The third transition region, which initiates at ~350 °C, is assigned to the degradation of alkyl chain moiety,[14] presumably leaving a stable SiO_X residue. The associated 77% weight loss corresponds closely to the theoretical value of 82% calculated for the loss of a $C_{18}H_{37}$ unit based on a molecular weight of 309. The final residual weight of ~17% observed at the highest temperatures corresponds to the contribution of 17.2% that would theoretically arise from a remaining SiOSi moiety.

(14) Wunderlich, B. *Thermal Analysis*; Academic Press: Boston, MA, 1990.

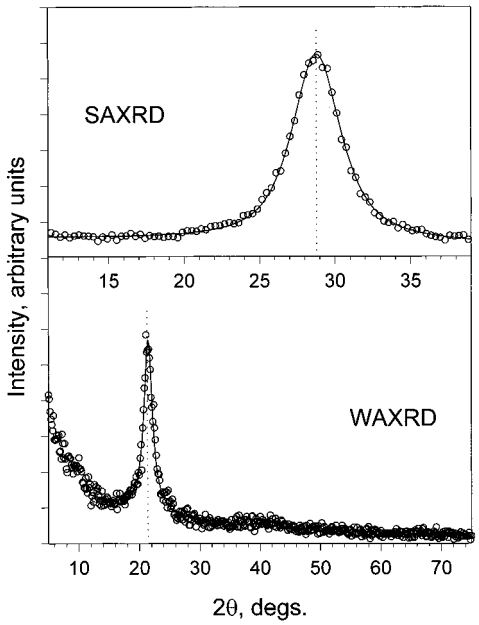

Figure 2. X-ray diffraction plots for powder samples of PODS. The top and bottom plots show the small- and wide-angle diffraction data, respectively. The experimental data are described by open circles (all data points not shown for clarity), the solid lines represent fits based on selected lineshape functions (details given in text) and the vertical lines are given as markers for the peak maxima.

3.2. X-ray Diffraction. 3.2.1. Wide Angle Diffraction. The WAXRD curve given in Figure 2 shows a single strong peak which can be closely fit using a mixed Gaussian (G) and Lorentzian (L) line shape function.[15] The best fit, shown in the figure, was observed for a 60% L function and exhibits a peak at 21.45° ($2\theta_B$) with a full width at half-maximum (fwhm) of 1.68°. A pure L function gives respective values of 21.44° and 1.56°, but the fit is poorer. Applying Bragg's Law,[16] $d = \lambda/(2 \sin \theta_B)$ with $\lambda = 1.5418$ Å, gives $d = 4.143$ Å, a value quite close to the chain−chain spacings observed in dense solid phases of alkyl chains, such as high surface pressure Langmuir monolayers of hydrocarbon-chain amphiphiles[17,18] and crystalline *n*-alkanes.[19,20] For example, Tippman-Krayer and Mohwald[17] have reported a chain spacing of 4.16 Å for an eicosanoic acid monolayer at the air−water interface with the chains packed in a dense (19.8 $Å^2$/molecule), distorted hexagonal phase. Also, Bohm et al.[21] report a chain spacing of 4.12 Å for cadmium triacontanoate [$(C_{29}H_{59}CO_2)_2Cd$] packed in a dense phase (18.4 $Å^2$/molecule) with a two-chain, rectangular unit cell.

(15) Wang, J.-I.; Harrison, I. R. In *Methods of Experimental Physics, Vol. 16B*; Fava, R. A., Ed.; Academic Press: New York, 1980.

(16) Klug, H. P.; Alexander, L. E. *X-Ray Diffraction Procedures For Polycrystalline and Amorphous Materials*; Wiley: New York, 1970.

(17) (a) Barton, S. W.; Thomas, B. N.; Flom, E. B.; Rice, S. A.; Lin, B.; Peng, J. B.; Ketterson, J. B.; Dutta, P. *J. Chem. Phys.* **1988**, *89*, 2257−2270. (b) Kjaer, K.; Als-Nielsen, J.; Helm, C. A.; Laxhauber, L. A.; Mohwald, H. *Phys. Rev. Lett.* **1987**, *158*, 2224. (c) Helm, C. A.; Mohwald, H.; Kjaer, K.; Als-Nielsen, J. *Biophys. J.* **1987**, *52*, 381. (d) Barton, S. W.; Thomas, B. N.; Flom, E. B.; Novak, F.; Rice, S. A. *Langmuir* **1988**, *4*, 233.

(18) Tippman-Krayer, P.; Mohwald, H. *Langmuir* **1991**, *7*, 2303−2306.

(19) (a) Ungar, G. *J. Phys. Chem.* **1983**, *87*, 689. (b) Doucet, J.; Denicolo, I.; Craievich, A.; Collet, A. *J. Chem. Phys.* **1981**, *75*, 5125.

(20) Ewen, B.; Strobl, G. R.; Richter, D. *Faraday Discuss.* **1980**, *69*, 19.

(21) Bohm, C.; Leveiller, F.; Jacquemain, D.; Mohwald, H.; Kjaer, K.; Als-Nielsen, J.; Weissbuch, I.; Leiserowitz, L. *Langmuir* **1994**, *10*, 830−836.

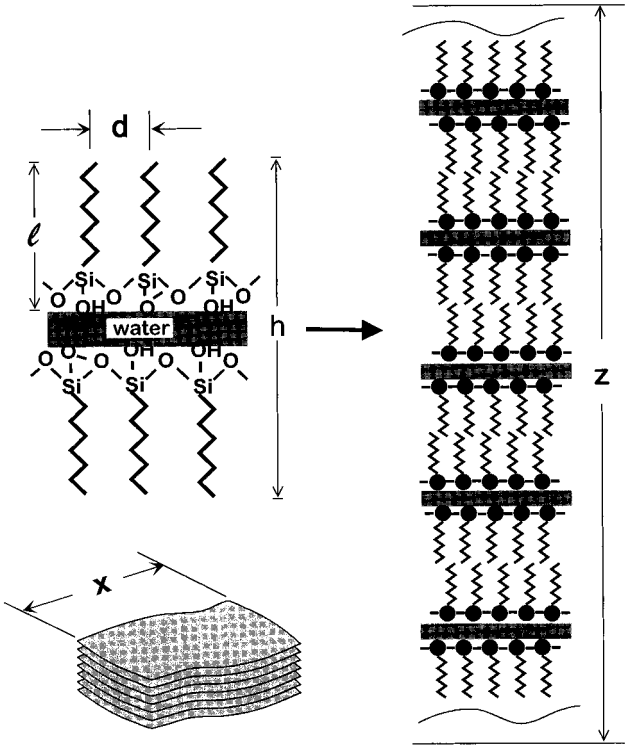

Figure 3. Schematic representations of the structure of the solid phase of PODS. The symbols *l*, *d*, *h*, *z*, and *x* represent the interchain spacing, extended ODS molecule length, ODS dimer unit distance including intercalated water, average correlation length of the crystalline layer stacks, and the dimension of a typical macroscopic crystallite of PODS, respectively. The corresponding values of the first four dimensions are 4.143, 26.2, 53.58, and 356 Å, respectively, based on small angle X-ray diffraction, molecular modeling, and wide-angle X-ray diffraction data, also respectively. For details, see text. Optical microscopy shows a distribution of sizes of roughly square flakes with $x \sim 10\ \mu$m as typical.

The surface densities of these phases correspond closely to the cross-sectional areas of the extended alkyl chains in lamellar *n*-alkane crystals.[20] Application of Scherer's equation,[22] given by

$$\tau = 0.9\lambda/B \cos \theta_B$$

allows calculation of the average correlation length of the Bragg planes, or, equivalently, the average crystallite size from the diffraction peak maximum position and the fwhm (in rad). Using the observed values of $\theta_B = 10.723°$ and $B = 0.029\,32$ rad, gives $\tau = 48.17$ Å. For the observed interplanar spacing of $d = 4.143$ Å, this value of τ corresponds to a translationally ordered organization of ~11−12 alkyl chains on average.

3.2.2. Small-Angle Diffraction. The SAXRD data are shown in Figure 2 as the top plot. The best fit to the broad line shape, also shown in the figure, was observed for an 80/20 L/G function with corresponding peak maximum and fwhm values of 28.779 and 3.899°, respectively. This peak maximum yields a Bragg spacing of 53.58 Å, which closely corresponds to the theoretical value of 52.4 Å predicted for the bilayer structure, $CH_3(CH_2)_{18}SiO_X-O_XSi(CH_2)_{18}CH_3$, from molecular models with a fully extended length of 26.2 Å for each alkylsiloxane unit. When the small- and wide-angle X-ray diffraction data are combined, the general structure of PODS is best represented as a stacked bilayer crystalline phase, shown in the representation in Figure 3. The observation of an ~1.2 Å larger stack spacing (*h* in Figure 3) than predicted from the model is consistent with the TGA data (see above) which indicate the presence of a single molecular layer of intercalated water in the SiO_X-SiO_X interface layer. Finally, the application of Scherer's equation to the diffraction data in Figure 2 gives an average crystallite size of ~356 Å (*z* in Figure 3), which corresponds to around seven correlated bilayer stacks.

(22) Cullity, B. D. *Elements of X-Ray Diffraction*; Addison Wesley: Reading, MA, 1978.

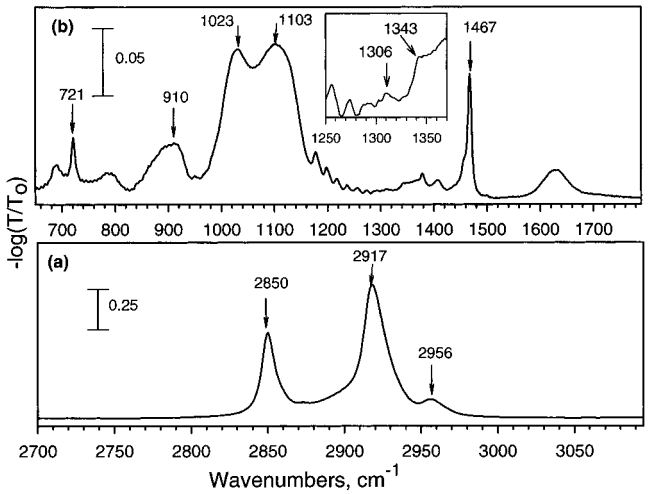

Figure 4. Transmission infrared spectra of a PODS sample dispersed in a KBr matrix. The inset shows an expanded spectrum of the 1250−1350 cm^{-1} region with arrows indicating the locations of peaks at 1310 and 1344 cm^{-1} which have been assigned tentatively as chain defect modes. For details see text.

3.3. Infrared Spectroscopy. 3.3.1. High-Frequency Region. The high-frequency transmission spectrum of PODS, given in Figure 4, shows the presence of four distinct peaks at 2849.4, 2872.6, 2917.5, and 2956 cm^{-1}, which are straighforwardly assigned to the CH_2 symmetric (d^+), CH_3 symmetric (r^+), CH_2 antisymmetric (d^-), and CH_3 asymmetric stretching (r^-) C−H vibrations, respectively.[23−25] The positions of the CH_2 mode peaks indicate the presence of high *trans* conformational populations of the alkyl chains because of the close correspondence of the frequencies to those reported for highly crystalline *n*-alkanes.[24] Further, the narrow fwhm values 11 and 15 cm^{-1} estimated for the d^+ and d^- modes are quite consistent with typically observed values for highly crystalline alkanes, for example, 8 and 13 cm^{-1}, respectively, for crystalline n-$C_{18}H_{38}$.[25]

3.3.2. Low-Frequency Region. SiO_X Modes. The peaks between 900 and 1100 cm^{-1} are characteristic of the siloxane group.[26] The singlet at 910 cm^{-1} is assigned to the Si−OH stretching mode;[26] its distinct presence establishes the presence of silanol groups and thus shows that the SiO_X network cross-linking is incomplete. The intense broad feature with maxima at ~1026 and 1100 cm^{-1} is assigned to the Si−O−Si antisymmetric stretching mode. In simple alkyldisiloxanes, the position of this peak typically is observed between 1020 and 1125 cm^{-1} with the exact position dependent upon the mass and the inductive character of the substituents. With progressively longer linear alkylpolysiloxane chains the absorption band splits into two or more overlapping components and in the limit of

(23) Dubois, L. H.; Nuzzo, R. G.; Allara, D. L. *J. Am. Chem. Soc.* **1990**, *112*, 558−569.

(24) (a) Snyder, R. G.; Schaachtschneider, J. H. *Spectrochim. Acta* **1963**, *19*, 85−116. (b) MacPhail, R. A.; Strauss, H. L.;Snyder, R. G.; Elliger, C. A. *J. Phys. Chem.* **1982**, *88*, 334−341. (c) Snyder, R. G.; Hsu, S. L.; Krimm, S. *Spectrochim. Acta, Part A* **1978**, *34*, 395−406. (d) Hill, I. R.; Lewin, I. W. *J. Chem. Phys.* **1979**, *70*, 842−581.

(25) Snyder, R. G.; Strauss, H. L.; Elliger, C. A. *J. Phys. Chem.* **1982**, *86*, 5145−5150.

(26) Bellamy, L. J. *The Infrared Spectra of Complex Molecules*; Chapman and Hall: London, 1975; pp 374−383.

very large chains appears as a broad feature between 1000 and 1100 cm^{-1} with maxima at ~1020 and 1086 cm^{-1}. Cyclic polysiloxanes, $[H_3CSiO(OH)]_x$, also absorb in this region. Trimers ($x = 3$) show a characteristic single band at 1020 cm^{-1}, tetramers and pentamers ($x = 4$ and 5) absorb typically at 1085 cm^{-1}, while even larger siloxane rings show gradually widening and band splittings. On this basis, the observed feature in Figure 4b is consistent with the formation of very long linear alkylpolysiloxane chains and/or a mixture of cyclic segments dominated by tetramers ($x \geq 4$) with a minor presence of trimers ($x = 3$).

Alkyl Chain Modes. The lowest frequency peak which appears at 720 cm^{-1} is assigned to the CH_2 rocking mode (P_1) vibration. Its appearance as a sharp [full width at half-maximum (fwhm) ~10 cm^{-1}] singlet at this frequency is characteristic of a crystalline chain packing in a triclinic or hexagonal structure.[27] We note that the introduction of internal kink defects, which serve to lower the number of correlated methylene units, will shift the peak to higher values, between 723 and 738 cm^{-1}, as well as increase the fwhm.[28] On this basis, we conclude that the alkyl chains in the PODS samples are quite highly organized. Further conclusions about the packing will be given below in the discussion of the 1467 cm^{-1} CH_2 scissoring deformation mode.

Starting from the high-frequency tail of the 1080 cm^{-1} siloxane stretching mode peak, a series of bands is observed between 1170 and 1380 cm^{-1}. This pattern of band progressions in the spectra of solid-phase alkyl compounds is attributed to coupled CH_2 wag modes (W_x), with the strongest intensities observed when a given chain is in an *all-trans* conformational sequence.[29] On this basis, we conclude that the low-frequency spectrum in Figure 4 establishes the presence of highly conformationally ordered, alkyl chains. In contrast, if the chains were disorganized, as in liquid-phase alkanes, these features would be smeared into a broad envelope. A further level of analysis is possible since the number and spacing of the W_x bands is directly related to the length of the *all-trans* conformational sequences.[30] In the present case of a terminally substituted alkyl chain, $CH_3(CH_2)_nX$, the interband spacing $\Delta\nu$ for an *all-trans* chain is related to the number of W_x modes below ~1350 cm^{-1} by the following equation:[31]

$$\Delta\nu = 326/(n + 1)$$

A 17 W_x band progression is expected for the present case of a fully extended $C_{18}H_{37}$ chain. Unfortunately, the broad tail of the antisymmetric Si−O−Si stretching absorption in Figure 4 precludes direct counting of all of these features. However, using an average value of $\Delta\nu = 19.5 \pm 0.5$ cm^{-1}, obtained over the spectral range between 1170 and 1275 cm^{-1}, the above equation gives a value of $n = 16$ (±0.2). On the basis of the theoretical value of 17 for a perfect *all-trans* chain, one can interpret this to mean that, on average, some fraction of terminal CH_2 units on an average chain exhibit a *gauche* conformation to leave a $-(CH_2)_{16}-$ *all-trans* sequence; equivalently, an ~[100 × (1/17) =] 5.9% average *gauche* population exists in the monolayer.

The appearance of very weak, yet distinguishable peaks at 1310 and 1344 cm^{-1} (see inset in Figure 4) is consistent with chain modes associated with localized *gauche* defects in the alkyl chain. In studies of the vibrational mode assignments for solid, crystalline odd *n*-alkanes, Maroncelli et al.[32] have attributed peaks appearing at 1345, 1353, and 1306 (as well as a weaker feature at 1366) cm^{-1} to wagging modes associated with end-*gauche* (*gtm*), double-*gauche* (*gg'tm*), and chain-kink (*tngtg'tm*) defects, respectively. On this basis, the weak peaks observed in our spectra at 1310 and 1344 cm^{-1} can be attributed to the presence a population of end-*gauche* and internal-kink defects in PODS. On the basis of well-established relative intensity correlations,[32b] we estimate the concentration of chain-end and internal-kink defects in the PODS samples to be in a narrow range of 2−10% per average chain, consistent with the estimate made above from the W_x bands. The small peak observed at 1378 cm^{-1} is assigned to the CH_3 symmetric bending (umbrella or U) mode. This mode can be considered as a local motion of the CH_3 group and therefore essentially independent of the conformation of the rest of the alkyl chain.

The sharp (fwhm ~8−10 cm^{-1}) peak at 1467.5 cm^{-1} in Figure 4 is straightforwardly assigned to the CH_2 scissoring deformation mode (δ), while the weak, but distinct, shoulder at ~1455 cm^{-1} is assigned to the CH_3 antisymmetric bending mode (α). The appearance of a singlet δ mode band implies the absence of factor group splitting, so there is essentially only one type of alkyl chain per unit subcell, while the small fwhm shows the presence of highly ordered, *all-trans* chains. In contrast, for conformationally *disordered* alkanes, fwhm values typically are ~18−25 cm^{-1}, significantly larger than observed. One likely possibility for the chain packing, consistent with the observed spectrum, is a phase II or rotator phase of a triclinic or hexagonal cell.[27] These phases consist of a single type of chain per unit subcell which undergoes hindered rotational and twisting motions about the long axis. The corresponding frequency and fwhm values of the δ mode are quite similar to what is observed in Figure 4b. In contrast, alkane phases exhibiting orthorhombic symmetry with two chains per unit subcell generally lead to doublet δ peaks because of interchain interaction, although this splitting can become negligible when the interchain spacing is sufficiently large.[33] However, since only a single, small interchain spacing is deduced from the WAXRD pattern (see above), this possibility seems unlikely and we conclude that the chains in PODS exist in a symmetrical hexagonal arrangement. We do note that it is also possible to consider a slightly distorted type of hexagonal packing, such as found in a triclinic arrangement of chains. The above analysis is completely consistent with the observation of a sharp singlet at 720 cm^{-1} for the P_1 mode (see above).

Finally, we note the peak at 1630 cm^{-1} which is assigned to the bending mode of water. While other evidence (XRD and TGA) indicates the intrinsic presence of monolayer quanitites of water in the PODS structure, the presence of adventitous absorbed water in the hygroscopic KBr matrix, in spite of our preparation protocol with dry KBr and oven-dried mixing vials, precludes a quantitative analysis for the water in PODS.

3.3.3. Comparison with Monolayer Spectra. In order to relate the structure of the $C_{18}H_{37}SiO_X$ moieties in PODS in a quantitative way to their structure in self-assembled ODS monolayers formed from OTS, previoulsy developed methods

(27) Snyder, R. G. *J. Mol. Spectrosc.* **1961**, *7*, 1161.
(28) Snyder, R. G.; *J. Chem. Phys.* **1967**, *47*, 1316−1360.
(29) (a) Jones, R. N.; McKay, A. F.; Sinclair, R. G. *Phil. Trans. R. Soc. Chem.* **1952**, *A74*, 2575−2578. (b) Brown, J. K.; Sheppard, N.; Simpson, D. M. *Phil. Trans. R. Soc. Chem.* **1957**, *A247*, 35. (c) Snyder, R. G. *J. Mol. Spectrosc.* **1960**, *4*, 411−434. (d) Snyder, R. G. *J. Chem. Phys.* **1967**, *47*, 1316−1358.
(30) Snyder, R. G.; Schaachtschneider, J. H. *Spectrochim. Acta, Part A* **1963**, *19*, 85−116.
(31) *Ibid.* **1963**, *19*, 117−168.
(32) (a) Maroncelli, M.; Qi, S. P.; Strauss, H. L.; Snyder, R. G. *J. Am. Chem. Soc.* **1982**, *104*, 6237−6247. (b) Snyder, R. G. *J. Chem. Phys.* **1967**, *47*, 1316−1360.
(33) (a) Chapman, D. *Trans. Faraday Soc.* **1965**, *61*, 2656. (b) Casal, H. L.; Mantsch, H. H.; Cameron, D. G.; Synder, R. G. *J. Chem. Phys.* **1982**, *77*, 2825.

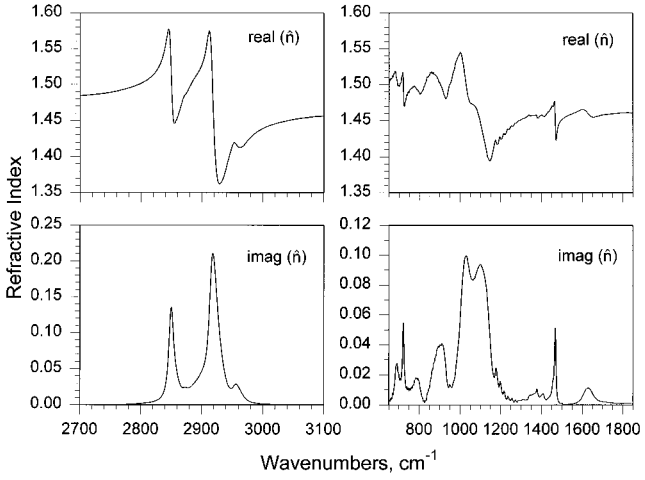

Figure 5. Optical function spectra of PODS obtained from transmission spectra of KBr dispersions (see Figure 4).

of spectral simulation were followed.[34] Since these methods have been described in considerable detail in the previous publication only a brief outline is given here. First, the intrinsic, isotropic IR optical function spectra, $\hat{n}(\nu) = n(\nu) + ik(\nu)$, of PODS were determined from transmission spectra of pressed KBr discs with known weight fractions of PODS dispersed in the matrix. The results are shown in Figure 5.[35] Next, the spectra were transformed into anisotropic optical function tensor spectra for different possible monolayer structures involving $C_{18}H_{37}SiO_X$ chains uniformly assembled with a single chain tilt angle, ϕ, defined relative to the surface normal, and a single twist angle of the C−C−C plane, θ, defined relative to the tilt plane. Finally, these simulations were compared to experimental monolayer spectra to find the closest fits. For this comparison, an ODS monolayer was formed by self-assembly of OTS on a prehydrated SiO_2/Si substrate according to previously described methods.[1d] The experimental transmission monolayer spectrum in the C−H stretching region is shown in Figure 6 (solid line) along with the best-fit simulation (dotted line) generated for a monolayer with ϕ and $\theta = 11$ and 46°, respectively. These values agree with the picture of a densely packed ODS monolayer approaching perfect hexagonal packing with near vertical chains. The strong correspondence in the intensities, linewidths and peak frequencies further shows that the inherent chain structure in PODS is strikingly similar to that in the self-assembled ODS monolayer on SiO_2. In addition, since the intrinsic IR frequency optical functions for the chain vibrational modes of substituted *n*-alkanes are strongly influenced by the exact nature of the substituent,[36] the observed transferrability of the optical constants of PODS to monolayer assemblies strongly suggests that the arrangements of the siloxy [SiO_X-$(OH)_Y$] species also must be highly comparable in the two cases. A similar comparison has been presented recently in a preliminary account of the effects of substrate on the monolayer structure, but details of the structure of PODS, used as the basis for the simulations, were not given.[1c] Similar simulations for the low frequency modes were not performed since there are a large number of overlapping peaks and assignment of peak components to specifc modes with reliable transition moment directions is difficult. Such analyses are in progress and will be reported elsewhere.

3.4. Nuclear Magnetic Resonance. The ^{29}Si resonances observed at −48.5, −57.4, and −69.0 ppm in Figure 7a can be

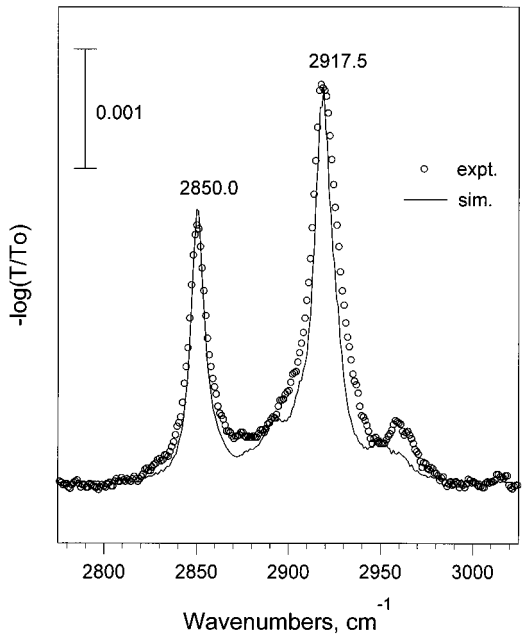

Figure 6. Simulated (solid line) vs experimental (circles) transmission spectra for a monolayer of octadecylsiloxane prepared by self-assembly on the pre-wetted surface of a native oxide film on silicon. The film was prepared according to the previously reported procedure in ref 1d, and the simulation was based on the optical function spectrum of PODS shown in Figure 5.

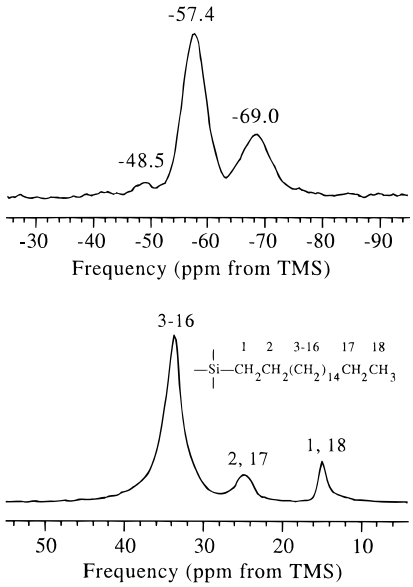

Figure 7. (A) ^{29}Si single-pulse MAS NMR spectrum of poly(octadecyl)siloxane, obtained with 1H decoupling during signal acquisition, a 50 s recycle delay, 975 scans, an exponential broadening of 40 Hz, and a 5.5 μs 90° pulse width. (B) ^{13}C CP MAS NMR spectrum of PODS, obtained with a 4 s recycle delay, 32 scans, an exponential broadening of 20 Hz, a contact time of 2 ms, and a 5 μs 90° pulse width.

associated, respectively, with the general alkylsiloxane structures $(HO)_2(R)Si(OSi)$ [geminal silanol], $(HO)(R)Si(OSi)_2$ [isolated silanol], and $(R)Si(OSi)_3$ [siloxane], where R = alkyl. The [siloxane]/[isolated]/[geminal] population ratios were determined to be 19.5/58.5/1.0 or, equivalently, 24.7, 74.1 and 1.3%, respectively, from the integrated peak area ratios.[37] The absence of resonances corresponding to sites where there are no Si−O−Si linkages implies that all of the Si atoms are involved in

(34) Parikh, A. N.; Allara, D. L. *J. Chem. Phys.* **1992**, *96*, 927−945.
(35) Digitized optical function spectra are available upon request from D.L.A.
(36) Shi, J. M.S. Thesis, The Pennsylvania State University, 1992.
(37) Glaser, R. H.; Wilkes, G. L.; Bronnimann, C. E. *J. Non-Cryst. Solids* **1989**, *113*, 73−87.

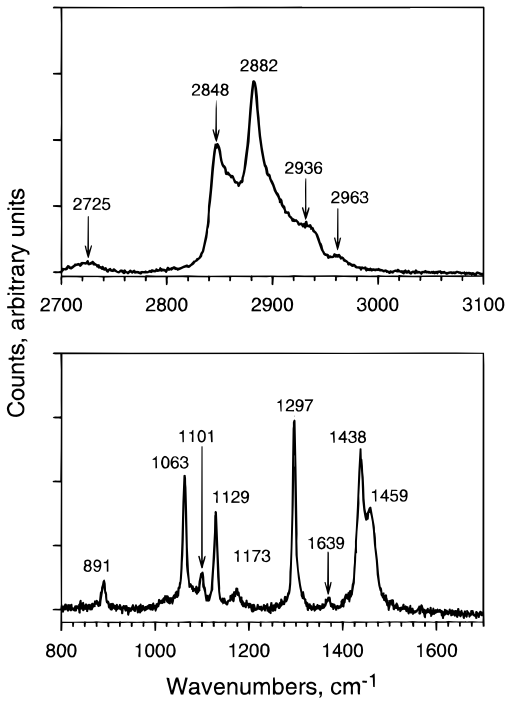

Figure 8. Raman spectrum of a bulk sample of PODS taken with excitation at 530.9 nm.

some degree of Si−O−Si cross-linking. The observation of a sizeable population of silanol-bearing sites indicates incomplete cross-linking of the SiO_X network and the high proportion of isolated silanols shows that the majority of Si atoms exhibit two cross-links. The latter characteristic would be consistent with a general structure consisting of extended linear siloxane chains and/or rings.

The ^{13}C resonances are shown in Figure 7b. The most intense peak at 34 ppm is assigned to the 14 CH_2 carbons (positions 3−16) in the $C_{18}H_{37}$ chain. The downfield shift of the resonances of these interior carbons relative to the corresponding values for a liquid-phase alkane with equilibrium populations of *trans* and *gauche* conformations (∼30 ppm) is taken as evidence for *all-trans* conformation chains,[38] consistent with the conclusions given in an earlier solid state NMR study of self-assembled monolayers on silica colloids.[5,39] The four remaining carbon environments at chain positions 1, 2, 17, and 18 are assigned to the peaks at 25 ppm (2, 17) and 15 ppm (1, 18).

3.5. Raman Spectroscopy. The Raman C−H stretching mode spectra are given in Figure 8. The C−H stretching mode features, shown in the high-frequency plot, give essentially the same information as given by the corresponding IRS data in Figure 4 and will not be discussed further. In contrast, the low-frequency Raman spectra provide details on the chain conformation which are not available from the IRS spectra. In a recent study of alkylsiloxane monolayers,[40] Thompson and Pemberton reported a Raman spectrum for a hydrolyzed ("gelled") bulk OTS sample which shows a near exact match to the one in Figure 8. Thompson and Pemberton concluded that the alkyl chains in their sample are essentially in *all-trans* conformations on the basis of two significant changes they observed in the spectrum of hydrolyzed OTS relative to that of the liquid state: (1) a large enhancement of the intensity ratio of the C−C stretching mode features associated with *gauche* and *trans* bonds [ν(C−C)*g* and ν(C−C)*t* bands, respectively] and (2) a narrow band shape and 7 cm^{-1} lower peak frequency of the CH_2 twist mode. These conclusions are directly applicable to our spectrum where one observes a narrow, symmetric peak at 1297 cm^{-1} for the CH_2 twist mode and an apparent absence of the ν(C−C)*g* relative to the ν(C−C)*t* peaks at 1180 cm^{-1} and 1063, 1129 cm^{-1}, respectively. These observations definitively confirm the IRS assignment of highly *trans* chains. In addition, the Raman spectrum (Figure 8) shows a narrow doublet with components at 1438 and 1459 cm^{-1}. The former is assigned to the CH_2 scissoring mode and the latter to the CH_3 antisymmetric bending mode.[41] Since our spectrum shows no features near 1418 cm^{-1}, the typical indication of an orthorhombic subcell packing,[42] it is likely that the chain packing in PODS involves some type of hexagonal subcell.

4. Discussion

4.1. Structural Summary. The wide variety of characterization data presented uniformly show that the structure of poly(octadecylsiloxane) consists of bilayered stacks of highly *trans* $C_{18}H_{37}$ chains, in which each layer exhibits a translational chain ordering and in which the interiors of the bilayers consist of a pair of parallel, cross-linked $SiO_X(OH)_Y$ sheets. This general structure is consistent with the features implied by the schematic in Figure 3.

The presence of high *trans* conformer populations in the alkyl chains is unambiguously established by the IR and Raman spectroscopic data and is indirectly implied by the XRD data which provide bilayer stack spacings of 53.58 Å, a value within 1.2 Å of twice the extended chain length of a $C_{18}H_{37}SiO_X$ unit (26.2 Å), and chain−chain spacings of 4.143 Å, a value within the range observed for dense crystalline alkyl phases. The IRS and Raman data are fully consistent with a hexagonal type of chain subcell. Finally, the XRD data show that the crystal domains are not large, with correlation lengths of the bilayer structure on the order of around seven stacks and correlation of the chain−chain packing on the order of ∼11−12 chains.[43]

The interior siloxy bilayer is shown by the ^{29}Si NMR data to consist of cross-linked $(-SiO)_X(OH)_Y$ sheets with relative populations of ∼25, 75, and 1% for Si atoms with $Y = 0$, 1, and 2, respectively. The significant presence of SiOH moieties is confirmed by appearance of characteristic SiOH vibrations in the IRS spectrum and establishes that the siloxy network is incompletely condensed. In addition, the IRS data suggest that the siloxy network consists primarily of long, linear, and/or cyclic polyalkylsiloxane segments with at least four repeat units. Both of these structures are consistent with the significant presence of ≡SiOH moieties. The presence of the strongly hydrogen bonding SiOH groups would indicate a tendency for absorption of water molecules and both the TGA and XRD data

(38) William, E. L.; VanderHart, D. L. *Macromolecules* **1979**, *12*, 762−767.

(39) The study of Gao and Reven, ref 4, reports solid-state ^{13}C and ^{31}P CPMAS NMR results on SAMs of octadecylsiloxane and zirconium octadecylphosphonate monolayers formed on nonporous, fumed silica and monodispersed silica colloids. They report an intense peak at 33 ppm, characteristic for a methylene carbon in an *all-trans* chain, and a much weaker peak at 30 ppm, characteristic for methylene carbons in disordered sequences. Their conclusion is that the ODS monolayers on the colloids are predominantly ordered, but less so than those typically reported on planar silica substrates, and are composed of coexisting domains of *all-trans* chains and of disordered chains.

(40) Thompson, W. R.; Pemberton, J. E. *Anal. Chem.* **1994**, *66*, 3362−3370.

(41) Lin-Vien, D.; Clothup, N. B.; Fateley, W. G.; Grasselli, J. G. *The Handbook of Infrared and Raman Characteristic Frequencies of Organic Molecules*; Academic: San Diego, CA, 1991; pp 9−25.

(42) Koenig, J.; Boerio, F. J. *J. Chem. Phys.* **1970**, *52*, 4826.

(43) Preliminary attempts to grow larger single crystals by solution recrystallization as well as by control of pH and temperature during the synthesis stage were unsuccessful. Further work is in progress along these lines.

are consistent with this conclusion. The former indicates incorporation of around one physisorbed H_2O per chain, or two molecules per chain bilayer. This conclusion is consistent with the XRD observation of an ~1.2 Å larger spacing of the chain bilayer stack than expected solely from twice the extended chain length of the $C_{18}H_{37}SiO_X$ unit. We note the interesting point that the dehydration behavior of the PODS siloxy structure is quite different from that of the surface of typical bulk silica. While both cases involve easily desorbed, physisorbed water, the silanol condensation processes differ as shown by the observation that the last vestiges of water release occurs from silica surfaces can occur at temperatures greater than 600 °C.[44] In contrast, in the present case, all water, both physisorbed and silanol condensate, appears to be released below the much lower temperature limit of ~160−170 °C. We speculate that, unlike the rigid surface of bulk silicas, the quasi-planar siloxy backbones in PODS are more readily deformed under thermal stress thereby allowing nonplanar SiO_X structures to form via silanol condensation at lower temperatures than in the rigid silica cases.[45]

The above structure represents a significant departure from the varieties of typical structures which have been reported for the hydrolysis of monoalkylsilanes, $RSiX_3$. In particular, it is well-documented[7] that random and cage structures, as determined by the nature of R, form for the cases of R = CH_3, CH_2-CH_3, or C_6H_5. Outside of the cursory reports mentioned earlier,[3,4] the only study of large monoalkyl silanes appears to be that of Adrianov and Izmaylov.[46] In this study, hydrolytic condensation of higher (C8−C10) alkyltrichlorosilanes upon subsequent dehydration was shown to yield low molecular weight (degree of polymerization = 6−8), stable silsesquioxanes with cubic molecular structures.

4.2. Mechanism of Formation and Implications for Monolayer Self-Assembly. On the basis of the extensive previous work in the area of silsesquioxanes, discussed briefly above, it is apparent that the incorporation of long alkyl chains, of the order of C18, drives the hydrolysis of $RSiX_3$ compounds toward formation of bilayer stacks, consistent with the increased van der Waals packing obtainable from the increasing of the chain length well above the previously studied range of C10 and lower. Thus, in spite of the significant thermochemical stability of a highly formed Si−O−Si network, the packing of the chains into a typical crystal habit, presumably hexagonal, is allowed to proceed during the assembly process to result in a bilayer structure, one of the three canonical aggregation geometries of amphiphilic surfactants (the others are spherical and cylindrical micelles).[47] The appearance of the bilayer pattern signals the dominance of chain−chain interactions in controlling the structural habit in PODS samples rather than the random template expected from Si−O−Si cross-linking forces. It is apparent then that the onset of significant cross-linking must lag behind the self-organization of alkyl chain bilayers in the PODS formation mechanism. This behavior in turn reveals significant insight into the PODS self-assembly mechanism, in particular, that the structure, growth, and stability are strongly directed by the well-understood thermodynamics of amphiphilic aggregation.[47,48] In this regard, one can access rich parallels with the self-organization of many amphiphiles including, most notably, phospholipids and certain surfactants, that spontaneously adopt a bilayer geometry in aqueous phases. Mechanistically and kinetically, the present structural data imply that the polymerization proceeds via a rapid, preliminary hydrolysis of OTS to form the surfactant species $RSi(OH)_3$, indicated in reaction 1 below, followed by a chain bilayer self-organization process, shown in reaction 2, which must occur significantly faster than the Si−O−Si condensation. Finally, this organized assembly can slowly undergo Si−O−Si condensation, via reaction 3, in a manner which is compliant with the preorganized chain template.[49] In contrast, if siloxy condensation were to precede by sequential Si−O−Si polymerization steps, as shown by reactions 4 and 5, one would expect the relative randomness and high stability of the Si−O bond network formed to preclude any extended correlation of chain organization and thus lead to an amorphous polymer.

$$RSiCl_3\ (liq) + H_2O \rightarrow RSi(OH)_3\ (aq) + HCl\ (aq) \quad (1)$$

$$n RSi(OH)_3\ (aq) \rightarrow [RSi(OH)_3]_n\ (bilayer) \quad (2)$$

$$[RSi(OH)_3]_n\ (bilayer) \rightarrow [RSiO_X(OH)_Y]_n\ (bilayer\ PODS) + zH_2O \quad (3)$$

$$2RSi(OH)_3\ (aq) \rightarrow R(HO)_2SiOSi(OH)_2R\ (aq) \quad (4)$$

$$RSi(OH)_3\ (aq) + [R(HO)_2Si]_2O\ (aq) \xrightarrow{polymerization} (amorphous\ PODS) \quad (5)$$

The essence of the mechanistic sequence embodied in reactions 1−3 is essentially the same as that proposed[1c,d] to rationalize the high degree of chain organization which can occur during the self assembly of long-chain silane monolayers on hydrophilic substrates pre-wetted with water.[50] The key proposed feature is the ability of surface-adsorbed $RSi(OH)_3$ surfactant species to undergo rapid lateral diffusion on a molecularly thin water film adsorbed on the substrate surface. Given sufficient mobility, the chains will then approach an organized structure, driven primarily by the maximizing of the chain packing, before significant Si−O−Si cross-linking sets in. This approximate parallel between bulk, 3-D assembly during hydrolysis and surface, quasi-2-D assembly on a water layer is considerably strengthed by the observation that the detailed chain structures of the 3-D crystalline samples of PODS and corresponding ODS monolayers supported on high-energy oxide surfaces appear virtually identical. Of specific significance is the ability of the IRS optical function spectra of PODS (Figure 5) to serve as a quantitative basis for the simulation of the observed experimental spectrum of a monolayer self-assembled from OTS on SiO_2 (Figure 6). This result shows the close correspondence of the two forms of assembled $C_{18}H_{37}$-SiO_X units. It thus appears from the above comparisons between

(44) Morrow, B. A.; Devi, A. *Trans. Faraday Soc.* **1972**, *68*, 403−409.

(45) Consistent with this picture, from temperature-dependent IRS spectra we observe a disordering of the PODS alkyl chain structure at temperatures well below 160−170 °C, accompanied by both a parallel diminution and rise of Si−OH and Si−O−Si stretching mode peak intensities, respectively. See ref 12.

(46) Adrianov, K. A.; Izmaylov, B. A. *J. Organomet. Chem.* **1967**, *8*, 435−441.

(47) See, for example: Gelbert, W. M., Ben-Shaul, A., Rouz, D., Eds. *Micelles, Membranes, Microemulsions, and Monolayers*; Springer: Berlin, 1994.

(48) Knobler, C. M.; Desai, R. C. *Annu. Rev. Phys. Chem.* **1992**, *43*, 207−236 and selected references cited therein.

(49) The detailed structure and degree of polymerization of the SiO_x network, however, is complicated and is expected to be determined by a subtle interplay of the reactivities of the terminal silanols on the condensing siloxy chains as well as the local solution environment, especially pH. Under our conditions, HCl is released (reaction 1) creating an acidic pH. Alteration of this pH could be expected to introduce some changes in the siloxy microstructure, e.g., the acylic and cyclic segment composition, and the crystallite size. Studies are in progress in our laboratory to explore such effects.

(50) Parikh, A. N.; Liedberg, B.; Atre, S. V.; Ho, M.; Allara, D. L. *J. Phys. Chem.* **1995**, *99*, 9996−10008.

quasi-2-D and 3-D assembly that the key feature is the *approach* of the system to a limit of free assembly of an intermediate surfactant-like species, e.g., $C_{18}H_{37}Si(OH)_3$, at an aqueous interface. In this limit specific film growth characteristics can be expected. In particular, an unconstrained bilayer system will follow a quasi-2-D growth along the lateral edges.[51,52] Further mesoscale organization of individual bilayers into a larger bilayer stack or into closed form vesicular shapes will then be driven by the minimum free energy structures accessible under the specific conditions. Further studies using a variety of spectroscopic and imaging probes are now underway in our laboratory to investigate the interrelation between the growth mechanisms in the 2- and 3-D self-assembling layered alkylsiloxane structures.

Finally we address very briefly analogies with other organic−inorganic materials. The long-chain poly(*n*-alkylsiloxane) compound in the present study belongs to a large family of diversely structured silsquioxane compounds[5,6] and brings to this family a new example of crystalline layered structures.[53] Within this larger family, several related organic−inorganic heterolayered structures have been prepared from co-condensation of anionic silicates and cationic surfactant molecules in what is generally referred to as a cooperative organization or templated condensation of the inorganic phase onto pre-formed organic assemblies.[54] We note that, in the formation of the presently studied layered organosilicates, the organization of the mesostructures is not guided by any ionic or electrostatic interactions between the siloxy head groups but rather is driven by the chain−chain interactions, aided by the entrained water phase, with a final cross-linking of the siloxy groups providing mainly an overall stability to the assembly. This type of sequential process has parallels with the widely studied family of layered alkylzirconium phosphates and phosphonates where layering is anchored at prefabricated structured sheets of $Zr(O_3POR)_2$ and $Zr(O_3PR)_2$ networks, respectively.[8−10] We also note that analogies between 2- and 3-D assemblies can be found in non-silicate systems. The primary example is the case of coinage metal alkanethiolates[55,56] (e.g., AgSR) where the self-organization of the alkyl tails, coupled with formation of covalent metal-SR bonds, leads to layered, organic−inorganic heterostructures. Direct comparisons of the structural attributes of these three classes of Zr-, Ag-, and Si-based structures for the same alkyl chain lengths are of significant interest within the context of the issue of the correlations of chain organization characteristics with structure dimensionality, and such studies are now in progress.

Acknowledgment. The authors acknowledge valuable discussions with F. Rondelez and W. Birch. Financial support was obtained from the National Science Foundation (DMR-900-1270, D.L.A. and A.N.P.; REU for M.A.S.) and the Advanced Projects Research Agency under the ULTRA initiative (ONR#9314426).

JA963284P

(51) Gelbert, W. M.; Ben-Shaul, A. *J. Phys. Chem.* **1996**, *100*, 13169−13189.

(52) Along these lines we note that a very recent *in-situ* atomic force microscopy study reports the observation of the coalesence of small domains into larger ones during alkylsiloxane monolayer growth. [Woodward, J. T.; Schwartz, D. K. *J. Am. Chem. Soc.* **1996**, *118*, 7861−7862].

(53) We also have sucessfully prepared other bilayered polyalkylsiloxane compound by hydrolysis of alkytrichlorosilanes for C12−C20 chains. All of these show conformational ordering by IRS but, as expected, the longer chains show higher ordering. These results will be reported elsewhere.

(54) Firouzi, A.; Kumar, D.; Bull, L. M.; Besier, T.; Sieger, P.; Huo, Q.; Walker, S. A.; Zasadzinski, J. A.; Glinka, C.; Nicol, J.; Margolese, D.; Stucky, G. D.; Chmelka, B. F. *Science* **1995**, *267*, 1138−1144 and selected ref. therein.

(55) (a) Dance, I. G.; Fisher, K. J.; Banda, R. M. H.; Scudder, M. L. *Inorg. Chem.* **1991**, *30*, 183. (b) Baena, M. J.; Espinet, P.; Carmen Lequerica, M.; Levelut, A. M. *J. Am. Chem. Soc.* **1992**, *114*, 4182−4185.

(56) Parikh, A. N.; Cutts, R. W.; Rubin, S.; Strouse, G.; Zawodzinski, T. A., Jr.; Swanson, B. I. Manuscript in preparation.